Advances in Water Resources 120 (2018) 98–113

Contents lists available at ScienceDirect

Advances in Water Resources

journal homepage: www.elsevier.com/locate/advwatres

Experimental investigation on dispersion mechanisms in rigid and flexible vegetated beds

Francesca De Serio[a,*], Mouldi Ben Meftah[a], Michele Mossa[a], Donatella Termini[b]

[a] Department of Civil, Environmental, Land, Building Engineering and Chemistry, Polytechnic University of Bari, Italy
[b] Dipartimento di Ingegneria Civile, Ambientale, Aerospaziale, dei Materiali, University of Palermo, Italy

ARTICLE INFO

Article history:
Received 8 December 2016
Revised 2 August 2017
Accepted 14 August 2017
Available online 16 August 2017

keywords:
Rigid vegetation
Flexible vegetation
Turbulent length
Dispersion
Advective transport

ABSTRACT

Vegetation in channels strongly affects flow structure and turbulence, with consequences on the hydrological storage of nutrients and chemical tracers, the shelter of stream biota as well as the trapping or transport of sediments. At the same time, all these phenomena are inevitably subjected to alteration of hydrological conditions in fluvial systems due to climate change. The present study intends to provide a thorough investigation into the processes of transport and dispersion induced by flow turbulence within the vegetation structure. Specifically, velocity measurements in vegetated channels were intensively conducted and analyzed in the case of both flexible submerged and rigid emergent canopies. The experiments aimed to: (i) highlight the differences in the hydrodynamic structures induced by different plant types and configurations; (ii) study the spatially varying dispersive properties and turbulent behavior of the current, attributable to different plant density, submergence and stiffness. Further, the spatial variability of velocity and turbulence distributions was taken into due consideration. The experimental results showed how longitudinal and transversal hydrodynamics and transport differ, depending on vegetation configuration and stem properties.

© 2017 Elsevier Ltd. All rights reserved.

1. Introduction

River vegetation has historically been acknowledged, from a hydraulic perspective, as a source of flow resistance, by increasing bottom roughness, decreasing near bed turbulent stress and reducing conveyance capacity (Gurnell, 2014; Nepf, 2012a, 2012b). Nevertheless, the reduced velocity and transport within the vegetation shelters biota, promotes the trapping of sediments as well as the storage and retention of nutrients, chemical tracers and microbes inside the canopy, also allowing flood control (Costanza et al., 1997; Kemp et al., 2000; Marois et al., 2015). Only recently, vegetation has been considered as an integral part of a river system. Its pivotal role in regulating ecological services and protecting from flood/drought risks has received remarkable attention (Nepf, 2012a; Pollen and Simon, 2005), considering that the alteration of hydrological conditions is strictly sensitive to climate change.

Mean and turbulent flows, advection and dispersion are perturbed by the canopy (Ben Meftah et al., 2014; Ghisalberti and Nepf, 2004; Ikeda and Kanazawa, 1996; Raupach and Thom, 1981). At the same time, varying water loads and flow characteristics affect the hydraulic behavior and resisting force of plants in a community, depending on their shape, stiffness, submergence, permeability/porosity, phenologic stage (growth, maturity, decay periods). The residence time, transport and fate of contaminants, nutrients, dissolved oxygen and other scalars, along with the deposition of sediment grains, can be accurately envisaged depending on our ability to understand the mechanism of exchange between the free stream and the vegetated region. Such a transfer mechanism is critical to the overall dispersion and seems primarily controlled by the canopy density and geometry (Ghisalberti and Nepf, 2005; Nepf, 2012b; Nepf et al., 2007; Oldham and Sturman, 2001; Poggi et al., 2009; Schultz et al., 1995).

To optimize the ecosystem functions and define adequate sediment management, a better knowledge of the impact of the changing conditions on suspended sediment mechanisms should be attempted. Namely, a mutual feedback exerts between water flows, vegetation and sediments, so that the first fundamental step to recognize and manage the impact of climate change on riverine systems is to deduce the interaction between vegetation and river hydrodynamics. The interplay between flow and vegetation creates feedbacks to sediment deposition (Liu and Nepf, 2016), based on flow velocity and stem-generated turbulence. The deposition of

* Corresponding author.
E-mail address: francesca.deserio@poliba.it (F. De Serio).

http://dx.doi.org/10.1016/j.advwatres.2017.08.005
0309-1708/© 2017 Elsevier Ltd. All rights reserved.

fine sediment and organic material could benefit from the flow velocity reduction between the plants, whilst local soil erosion could diminish, due to the reduction of the bed shear stress (Crosato and Saleh, 2011; Righetti, 2008; Righetti and Armanini, 2002). In any case, when the main flow is diverted towards unobstructed areas, enhanced velocities laterally adjacent to the patch are produced, so that a transversal sharp transition region at the interface between the obstructed and unobstructed domains is formed. A transverse shear occurs, generating large-scale horizontal vortices centered around the edge of the vegetated area (Ben Meftah and Mossa, 2016; Ben Meftah et al., 2014; Lima and Izumi, 2014; White and Nepf, 2007a, 2007b), which might cause localized erosion (Liu and Nepf, 2016).

The effects of vegetation on the dispersion process have been experimentally investigated for both the submerged and emergent cases, but usually the cross section spatial averaging of non-uniform advection and diffusion results have been applied (Nepf and Vivoni, 2000; Nepf et al., 1997; Perucca et al., 2009). In this way, the variation of the transversal diffusion and advection cannot be examined.

Experiments by Nepf et al. (1997) within an array of emergent cylindrical rods using a continuous injection technique showed that, when plants are present, the vertical diffusivity and the diminished vertical shear reduced the shear-flow dispersion. The production of turbulence within a stand of emergent vegetation is dominated by the stem wakes rather than by the bottom-boundary shear, as in open-channel flows (Nepf et al., 1997). A relation between water depth and turbulence structure was highlighted by Nepf and Vivoni (2000), who pointed out that the generation of wake turbulence is strongly associated with the relative water depth. Analyses of velocity spectra and turbulent kinetic energy profiles showed that in natural river vegetation (Naden et al., 2006) and in model canopies (Ricardo et al., 2014; Zong and Nepf, 2012) stem-scale turbulence is absent at low stem Reynolds number Re_d and arises at $Re_d > 200$ (Nepf and Vivoni, 2000; Tanino and Nepf, 2008), with Re_d equal to the product of flow mean velocity and stem diameter rated by kinematic viscosity. In the case of rigid vegetation, Tanino and Nepf (2008) proposed a model for the mean turbulence intensity and the lateral dispersion coefficient due to the spatially heterogeneous velocity field, as a function of cylinder distribution and density. Their study proved that only turbulent eddies with mixing length scale greater than stem diameter contribute significantly to net lateral dispersion. Shucksmith et al. (2010) showed that, in emergent conditions, the mixing process dominant factor is the degree of reduction in spatial variation of velocity over the channel cross-section.

The effects of submerged vegetation on the longitudinal dispersion coefficient were investigated by Ghisalberti and Nepf (2006), who proposed a two-zone model to identify three contributing processes: large-scale shear dispersion above the canopy, inefficient exchange between the canopy and the overflow, and stem-scale dispersion within the canopy. Later, Shucksmith et al. (2011) utilized an empirical data set of longitudinal mixing measurements to evaluate the performance of both existing and newly proposed models for mixing in submerged vegetated open channel flow. They highlighted that the rate of mixing in such systems is dependent on the relative size of the flow layers, the difference in average velocity, and the rate of the vertical mass transfer.

Furthermore, the physical structure of individual plants and the canopy morphology alter the velocity field across several scales (Ben Meftah et al., 2014; Ben Meftah et al., 2015; Nepf, 2012a, 2012b; Tanino and Nepf, 2008), ranging from individual branches and blades on a single plant to a community of plants in a meadow or patch. Flow structure at different scales is relevant to different processes. As an example, the reteNepfntion and release of organic matter, mineral sediments, seeds, and pollen from a meadow or patch depend on the flow structure at the meadow or patch scale (Mossa and De Serio, 2016; Mossa et al., 2017). Literature shows that, with emergent vegetation the turbulent length scales are set by the stem diameter and spacing (see among others Ben Meftah and Mossa, 2013, 2012b, Nepf, 2012a; Tanino and Nepf, 2008; Termini, 2016a). Shucksmith et al. (2010) proved that in the presence of a relatively uniform distribution of plant blockage over the width and depth, mixing is dominated by stem scale processes. In the case of dense submerged vegetation, the drag discontinuity at the top of vegetation generates a shear layer with canopy-scale vortices controlling the exchanges of mass and momentum between the canopy and the overflow (Nepf, 2012a; Termini, 2015). Furthermore, the turbulent transport occurs inside the upper part of the vegetated layer.

Despite turbulent unobstructed flows (i.e. river and sea currents, jets) have been extensively studied (see among others Ben Meftah et al., 2017; Cuthbertson et al., 2006; De Serio and Mossa, 2014, 2015; Mossa, 2004), flows through regions with vegetation still deserve an in-depth examination. In fact, from the brief notes above described, it is evident that the knowledge of the 'engineering' role played by vegetation in regulating eco-services and river management is crucial, even if challenging. According to Gregory et al. (1991), Lotsari et al. (2015), Sandercock and Hooke (2011), modelling should play an important role in reducing uncertainty associated with channel sensitivity and responses to threshold conditions. Strategies for quantifying solute transport in vegetated rivers consist of lumped models (Ghisalberti and Nepf, 2005), upscaled models (Marion et al., 2008) and numerical solutions of the advection–dispersion equation (Rubol et al., 2016). However, the most relevant issue to both simulations and predictions is modelling calibration and validation. For this reason, since it is hard to monitor in-situ sediment/water interactions due to required timescales, laboratory experiments are needed to investigate transport patterns and dynamics for different vegetation scenarios.

Laboratory experiments in flumes provide the opportunity: (i) to evaluate the impact of different hydrodynamic regimes on different plant types and configurations, in controlled conditions (ii) to assess and estimate the action played by streamwise patterns of vegetation on the processes of transport and dispersion of turbulence and tracers in the three directions. The purpose of the present study is to analyze these two aspects, specifically considering the 3D spatial variability of the flow-canopy interaction. A simple analogy can be obtained relating the solute transport of the vegetated river with its sediment transport. In any case, the above-mentioned analogy involves the knowledge of key parameters governing the process such as grain size or settling velocity, thus it goes beyond the analysis of the present research.

Experiments were carried out in two different laboratory facilities and two different types of surrogate vegetation were used. The structure of the vegetation was simplified and attention was focused on the effect of its main parameters (i.e. vegetation stiffness, density and size) on the processes of turbulence transport and dispersion. To this aim, plant elements having the same characteristic dimension but a different stiffness were considered and the experimental runs were conducted for different plant submergences and plane distributions. Firstly, a sparse rigid and emergent canopy was studied in two different hydrodynamic configurations. After this, a dense, flexible and submerged canopy was investigated.

The present paper is structured in the following way. In the next section a theoretical background is provided to point out the principal variables involved in the process of turbulence and solute transport. In Section 3, the experimental work is illustrated, while results from the two canopies are analyzed in Section 4 and finally discussed in Section 5.

2. Theoretical approach

2.1. Main variables involved

A canopy consists of a distribution of plant elements. In the present paper both rigid cylinders of uniform diameter d and submerged canopy of blade width d were considered. Thus, according to Ghisalberti and Nepf (2009), it is reasonable to define d as the characteristic element scale within the canopy. Other key parameters characterizing the canopy are the solid volume fraction ϕ, i.e., the volume within the canopy occupied by solid elements, which is the complement of the canopy porosity $\eta = 1-\phi$ and the frontal area per unit length of the canopy $a = nd$, where n is the number of elements per unit planar area. In the case of a periodic square array of cylinders the value of a is equal to $1/s^2$, being s the axis-to-axis distance of the cylinders. Within the array the flow is spatially heterogeneous at the scale of the individual elements and often unsteady in time. Generally, in the case of obstructed flows the double-averaging method is used to remove the temporal and element-scale spatial heterogeneity of the current (Finnigan, 1985; Raupach and Shaw, 1982). In other words, the instantaneous equations of the vegetated current are first averaged over a time longer than the time scale of turbulence or instabilities in the flow and then averaged over an infinitesimally thin area that spans many cylinders, including only the area occupied by the fluid. In the present study, only the time-averaging procedure (indicated by the overbar sign) is used, to not miss information on the typical spatial variations in the longitudinal and transversal sections. For the sake of simplicity, the ambient current is considered uniform.

2.2. Solute transport and contribution from turbulence

Hereafter we consider a rectangular canopy located in a fluid of depth H. The canopy length is parallel to the mean flow directions with u, v and w the streamwise, transverse and vertical velocity components, respectively. The x-axis is parallel to the mean flow and sits along the centerline of the channel and array. The y-axis is at the leading edge of the canopy and is perpendicular to the mean flow direction. The profile of the current velocity upstream of the canopy is assumed uniform over the water depth.

The transport of a tracer c (species concentration) is described by the following expression:

$$\frac{\partial c}{\partial t} + \mathbf{v}\cdot\nabla c = -\nabla\cdot(-D_0\nabla c) \tag{1}$$

where t is time, $c(\mathbf{x},t)$ is the solute concentration, $\mathbf{v}(\mathbf{x},t)=(u,v,w)=(v_1,v_2,v_3)$ is the fluid velocity, D_0 is the molecular diffusion coefficient and $\mathbf{x}=(x,y,z)=(x_1,x_2,x_3)$. Neglecting the molecular diffusion, that is small in a turbulent flow, and time averaging Eq. (1) over a time interval much longer than the time scales of turbulent fluctuations, we have the time-averaged concentration equation

$$\frac{\partial \overline{c}}{\partial t} + \frac{\partial \overline{u_j}\,\overline{c}}{\partial x_j} = -\frac{\partial \overline{u_j'c'}}{\partial x_j} \tag{2}$$

where the overbar denotes the temporal average and the prime symbol denotes the temporal fluctuations, so that

$$\begin{aligned} c(\mathbf{x},t) &= \overline{c}(\mathbf{x}) + c'(\mathbf{x},t)\\ u(\mathbf{x},t) &= \overline{u}(\mathbf{x}) + u'(\mathbf{x},t)\\ v(\mathbf{x},t) &= \overline{v}(\mathbf{x}) + v'(\mathbf{x},t)\\ w(\mathbf{x},t) &= \overline{w}(\mathbf{x}) + w'(\mathbf{x},t) \end{aligned} \tag{3}$$

Eq. (2) shows that the concentration mass flux is due to the convection by the time-averaged flow (also named mean flow), $\overline{uc}$, $\overline{vc}$ and $\overline{wc}$, and transport by turbulent velocity fluctuations, $\overline{u'c'}$, $\overline{v'c'}$ and $\overline{w'c'}$.

Eq. (2) can be rewritten as follows:

$$\frac{\partial \overline{c}}{\partial t} + \frac{\partial \overline{u_j}\,\overline{c}}{\partial x_j} = K_{jj}\frac{\partial^2 \overline{c}}{\partial x_j^2}. \tag{4}$$

In fact, following Ting and Kirby (1995, 1996), in direct analogy to turbulent momentum transport, also turbulent mass concentration transport is assumed to be related to the gradient of the transported quantity. In this way, K_{jj} are the coefficients for net dispersion, which parameterize $\overline{u_j'c'}$, i.e. the turbulent diffusion.

Furthermore, the terms $\overline{u_j'c'}$, like the molecular diffusion, are expected to be Fickian if the spatial scale of the contributing mechanisms is smaller than the scale over which the mean concentration gradient varies. The mechanisms associated with the terms $\overline{u_j'c'}$ have characteristic scales of the stem diameter d and axis-to-axis distance s.

Differently from Tanino and Nepf (2008), who averaged Eq. (1) both in time and in space, in our present case the flow is three-dimensional and, therefore, the equations are only time-averaged. This means that the present study focuses on the turbulent diffusion, whereas the mechanical dispersion is the consequence of the time-averaged spatial fluctuations (Tanino and Nepf, 2008).

In the analysis of the flow-dispersion interaction, the turbulent kinetic energy (TKE) is important in determining the turbulent dispersion coefficient and thus the mass transport. The turbulent dispersion coefficient may be written as the product of a length scale and a velocity scale. A physical meaningful velocity scale is $\sqrt{k}$, where k is the turbulent kinetic energy, i.e.

$$\begin{aligned} k &= \overline{k'} = \frac{1}{2}\overline{u_i'u_i'}\\ k' &= \frac{1}{2}u_i'u_i' \end{aligned} \tag{5}$$

Therefore, the determination of the time and spatial variations of turbulent kinetic energy is of great importance in the evaluation of the dispersion process. For high Reynolds numbers the equation of the turbulent kinetic energy is

$$\begin{aligned} &\underbrace{\frac{\partial k}{\partial t}}_{\text{Local derivative}} + \underbrace{\frac{\partial \overline{u_j}k}{\partial x_j}}_{\text{Advection}}\\ &= -\frac{\partial}{\partial x_j}\left(\underbrace{\frac{1}{\rho}\overline{u_j'p'}}_{\text{Pressure diffusion}} + \underbrace{\overline{u_j'k'}}_{\text{Turbulent transport}}\right)\\ &\quad \underbrace{-\frac{1}{2}\overline{u_i'u_j'}\left(\frac{\partial \overline{u_i}}{\partial x_j} + \frac{\partial \overline{u_j}}{\partial x_i}\right)}_{\text{Production}} \underbrace{-\frac{1}{2}\nu\overline{\left(\frac{\partial u_i'}{\partial x_j} + \frac{\partial u_j'}{\partial x_i}\right)^2}}_{\text{Dissipation}} \end{aligned} \tag{6}$$

As shown by Nepf (1999), it reasonable to assume that the production term is of order of the dissipation term. Our experimental data and previous literature findings (Nepf, 1999; Nepf and Vivoni, 2000) enabled us to confirm this assumption. Namely, considering the production of TKE as the sum of wake and bed shear production terms, Nepf (1999) noted that, in the emergent case, the bed shear production is negligible over almost all the flow depth, apart from the zone very close to the bed. Consequently, TKE dissipation and wake production balance over almost all the flow depth, apart from the zone close to the bottom. In the submerged case, the shear at the top of vegetation could provide an important source of turbulence. Nevertheless, for shallow depth ratios and especially inside the vegetation, Nepf and Vivoni (2000) proved that the wake production is of order of the turbulence dissipation.

Furthermore, to obtain the diffusive transport terms, in turbulence modeling, turbulent diffusion is often assumed proportional

to the gradient of k (Rodi, 1984), i.e.

$$-\left(\frac{1}{\rho}\overline{u_j{}'p'}+\overline{u_j{}'k'}\right)=D_k\frac{\partial k}{\partial x_j} \tag{7}$$

with the turbulent diffusion coefficient D_k

$$D_k=\frac{\nu_t}{\sigma_k} \tag{8}$$

where ν_t is the eddy viscosity and σ_k is an empirical diffusion constant. Therefore, being energy dissipation and production of the same order of magnitude, the transport equation for k becomes

$$\frac{\partial k}{\partial t}+\frac{\partial \overline{u_j}k}{\partial x_j}=D_k\frac{\partial^2 k}{\partial x_j^2} \tag{9}$$

where, following the eddy-diffusivity concept (Nepf, 1999; Ting and Kirby, 1995), the turbulent diffusion coefficient is assumed as

$$D_k=l\sqrt{k} \tag{10}$$

with l the integral length scale associated with turbulent eddies. Eq. (9) is formally analogous to Eq. (4) and, therefore, assuming that the Prandtl number is $O(1)$, the analysis of the terms of Eq. (9) can be used for Eq. (4).

Consequently, it seems interesting to investigate the relations between $\overline{u}$, $\overline{v}$, $\overline{w}$ and k. In fact, the analogy between Eqs. (4) and (9) suggests that the cross-correlation between the time-averaged turbulent kinetic energy and the $\overline{u}$, $\overline{v}$ and $\overline{w}$ velocity components is related to the time-averaged solute concentration $\overline{c}$ transport by the mean flow, $\overline{uc}$, $\overline{vc}$ and $\overline{wc}$.

This approach was also used by Ting and Kirby (1994), who stated that the suspended sediment concentration shows that the mass flux along the flow direction is due to convection by mean flow and transport by turbulent velocity fluctuations, while the tendency of sediment to settle out is counteracted by the action of turbulent fluctuations. In their study, they proved that if it is assumed that turbulent velocity fluctuations are responsible for keeping sediment in suspension, and the mean flow transports the sediment, then suspended sediment transport resembles turbulence transport.

In the present study, sediments were not directly investigated and consequently some key parameters, like grain size or settling velocity, were not available to examine thoroughly the analogy between the transport of TKE and the sediment transport. In any case, the analogy between the transport of TKE and the transport of a scalar concentration by means of the mean flow is reliable and is taken into consideration, referring to both Eqs. (4) and (9).

The integral length scale l, present in Eq. (10), can be evaluated by the power spectrum or by multiplying the integral time scale T_u by the local time-averaged velocity $\overline{u_i(\mathbf{x})}$, where T_u is estimated by the autocorrelation function of the turbulent velocity fluctuations, i.e.

$$l_i=\overline{u_i(\mathbf{x})}\cdot T_u=\overline{u_i(\mathbf{x})}\cdot\int_0^{\tau_0}\frac{u_i{}'(\mathbf{x},t)\cdot u_i{}'(\mathbf{x},t+\tau)}{\overline{u_i{}'^2(\mathbf{x})}}d\tau \tag{11}$$

with τ the time lag with respect to t and τ_0 the value of τ at the first zero-crossing.

The integral length scale of turbulence l depends strongly on the presence of cylinders. In unobstructed flow, l increases with the scale of the diffusion patch until the largest length scale is reached, that is the length scale defined by the flow domain (Okubo, 1971). Emergent canopies impose structure on both the mean and turbulent flow over the entire water column. In flows with emergent vegetation, the canopy dissipates eddies with scales greater than the stem scale of s and d, while contributing additional turbulent energy at these stem scales. Thus, the dominant turbulent length scale within a canopy is shifted downward from analogous condition without vegetation. Particularly, in a channel with a regular array of cylinders, the integral length scale of the turbulence is set by the smaller of the stem diameter, d, or the distance between the stems s, regardless of the water depth (Taylor, 1935; Tanino and Nepf, 2008). In other words, for $d \le s$, turbulence is generated within stem wakes (if the Re_d is larger than 120) so that $l=d$; on the contrary, for $d>s$, turbulence is generated within the pore channels so that $l=s$.

These two depicted regimes in presence of cylinders are not exhaustive, since for low solid volume fractions (ad less than 0.01) the integral length scale of the turbulence should have an intermediate value between those previously mentioned, i.e. $l=O(\min(d,s)\div H)$. For further details, see for example Nepf et al. (1997) and Lopez and Garcia (1998).

Analogously to Eq. (10), Tanino and Nepf (2008) assumed that the net dispersion coefficients could be assumed equal to

$$K_{jj}=\alpha\sqrt{k}l_j \tag{12}$$

where the scale factor α could generally differ for horizontal and vertical diffusion. Following Nepf (1999), it is reasonable to assume the horizontal dispersion coefficient value in the range [0÷1].

3. Methods and materials

Literature (Nepf, 2012a) shows that aquatic plants exhibit a wide range of geometry and distribution. Marsh grasses are relatively sparse, with stem diameters $d=0.1\div1$ cm, $\phi=0.1\div1\%$, and $a=1\div7\ \mathrm{m}^{-1}$. Mangroves are among the densest canopies, with ϕ as high as 45%, mean trunk diameters of 4–9 cm, and a up to $20\ \mathrm{m}^{-1}$. Seagrasses have $a=1\div100\ \mathrm{m}^{-1}$ and $\phi=1\div10\%$. Emergent plants tend to have rounded stems for higher stiffness, and submerged grasses tend to have a blade geometry in which the width (0.3÷1 cm) is larger than the thickness (≈0.1 cm), in which case d is the blade width.

Based on the above information, two flow velocity datasets have been used in this work: the first one (herein indicated as BA-R data set) was collected with the bed covered by rigid emerged vegetated stems; the second one (herein indicated as PA-F data set) was collected with flexible and submerged vegetation on the bed. The manifest diversity of the two vegetated systems is justified by the aim to identify the key parameters which drive their different behaviors and find possible analogies in the hydrodynamic and dispersion processes. The vegetation elements were characterized by the same characteristic dimension d.

3.1. Setup and instrumentation for the rigid vegetated flume (BA-R data set)

Experimental runs were carried out in a smooth horizontal rectangular channel in the Department of Civil, Environmental, Land, Building Engineering and Chemistry of the Polytechnic University of Bari (Italy). The channel was 25.0 m long, 0.40 m wide and 0.50 m deep, with lateral walls and bottom surface in Plexiglas, as shown in Fig. 1. A stable recirculating flow was guaranteed in the channel. For details please refer to Ben Meftah and Mossa (2013) and Ben Meftah et al. (2015).

The vegetation array was constructed of vertical, rigid, circular steel cylinders, with threaded lateral surfaces and thus considered as rough cylinders. The cylinder diameter was $d=0.003$ m. The cylinder extremities were inserted into a plywood plaque 3.0 m long, 0.02 m thick and a width equal to those of the channels, which in turn was fixed along the channel bottoms, forming the experimental area. The plywood plaque was extended 3 m both upstream and downstream of the array of cylinders (experimental area) and was tapered to the channel bottom to minimize flow disturbance (Fig. 1). Cylinders were arranged regu-

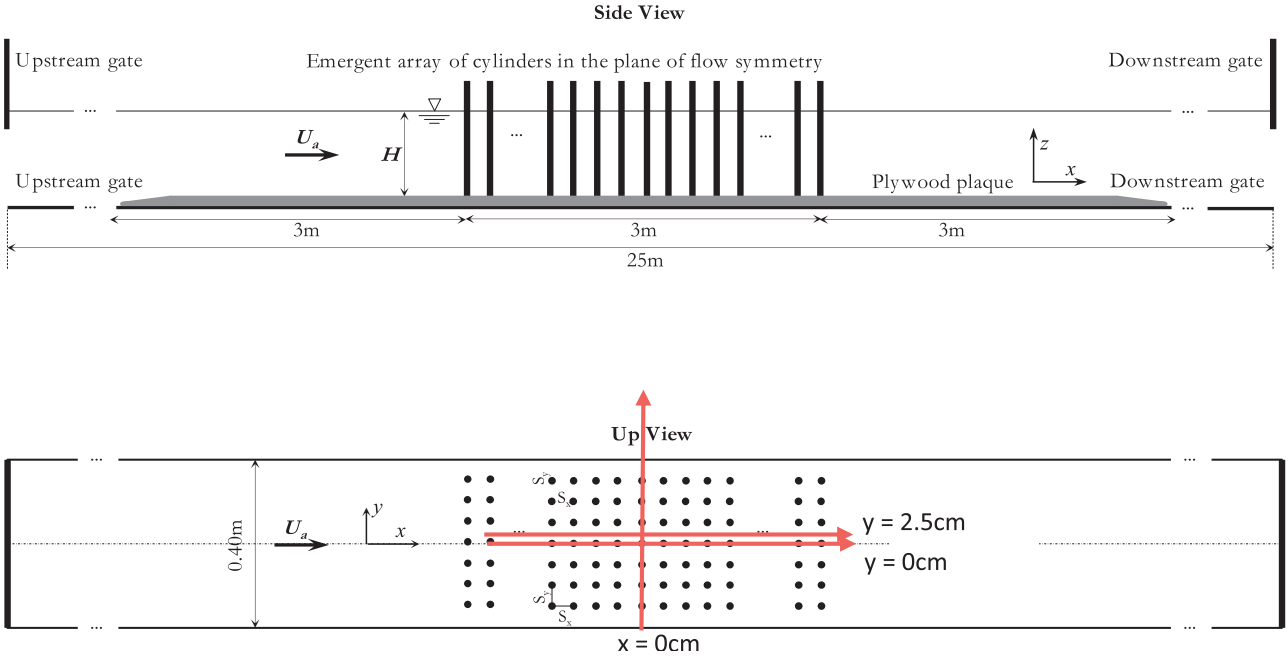

Fig. 1. Definition sketch of the channel with the array of cylinders. BA-R data set.

Table 1
Initial conditions and parameters of the experiments.

Run	H (m)	Q_a (m^3/s)	U_a (m/s)	Re_d	F_a	d (m)	a (m^{-1})
BA-R1	0.37	0.024	0.16	480	0.081	0.003	1.2
BA-R2	0.30	0.023	0.19	629	0.111	0.003	1.2
PA-F	0.11	0.035	0.82	2466	0.804	0.003	57

larly and spaced longitudinally and transversally with the same axis-to-axis distance $s = 0.05$ m, so that the cylinder density, n, was 4 cylinders/dm^2, while the vegetation density per meter was $a = 1.2$ m^{-1} and the solid volume fraction was $\phi = 0.28\%$. Therefore, following Nepf (2012a), this vegetation can be considered sparse.

A Cartesian coordinate system (x, y, z) was adopted, in the centre of the array, with x-, y- and z-coordinates denoting the longitudinal, transversal and vertical directions, respectively. Because water was forced to move around the cylinders, the flow within the canopy was turbulent and highly heterogeneous at the scale of the individual stem. Therefore, the instantaneous three-dimensional flow velocity components, through different longitudinal, cross and horizontal planes, were accurately measured (1cmx1cm grid resolution) using a down looking three-dimensional Acoustic Doppler Velocimeter (ADV)/Vectrino system by Nortek. The ADV was used with a velocity range equal to ±0.30 m/s, a velocity accuracy of ±1%, a sampling rate of 100 Hz and a sampling volume of vertical extend of 9 mm. The acquired data were filtered based on Tukey's method (Ben Meftah et al., 2015) and bad samples (signal-to-noise ratio SNR < 15 db and correlation coefficient < 70%) were removed. Measurements were carried out placing the ADV between two consecutive rigid stems.

Two different runs were analysed, with different flow depths and mean channel velocities, named BA-R1 and BA-R2. The initial experimental conditions and parameters of the runs are shown in Table 1. Herein, B is the channel width and $F_a = U_a/(gH)^{0.5}$ is the inlet flow Froude number, with $U_a (= Q/BH)$ the mean channel velocity, g the gravity acceleration and Q the flow rate. The element Reynolds number Re_d was calculated based on d and on the time-averaged velocity, also averaged in the transversal plane.

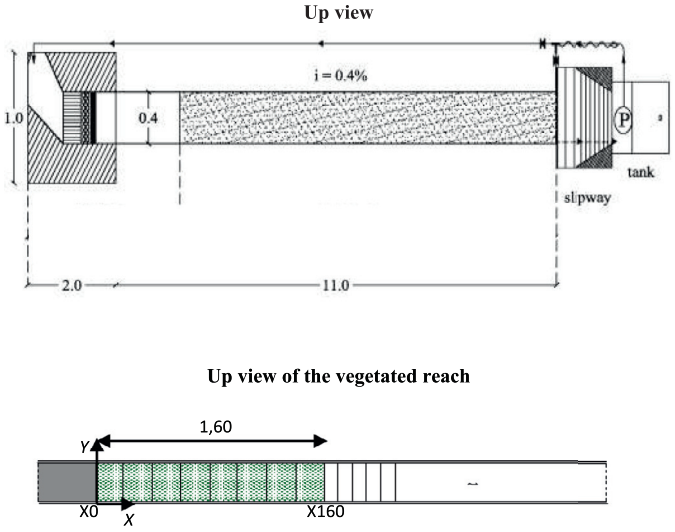

Fig. 2. Fig. 2. Definition sketch of the vegetated channel. PA-F data set. All measurements are in meters.

3.2. Setup and instrumentation for the flexible vegetated flume (PA-F data set)

The data used for such a comparison were collected in a straight laboratory channel constructed at the Hydraulic Laboratory of DICAM Department of University of Palermo (Italy). Details of the experimental apparatus can be found in previous works (Termini, 2013, 2016a; Termini and Sammartano, 2012). Thus, only information important for the following analysis is reported in this section. The rectangular flume was 11.2 m long and 0.4 m wide (see Fig. 2). The longitudinal bed slope was equal to 0.4% and the channel reach (1.60 m long) downstream of the initial section X0 (see Fig. 2) was covered by real herbaceous (flexible) vegetation (*Festuca arundinacea*). The vegetation stems had a blade geometry with width $d = 0.003$ m. The blade width was obtained as average value of 15 measures in 10 samples of unit area (dm^2). The experimen-

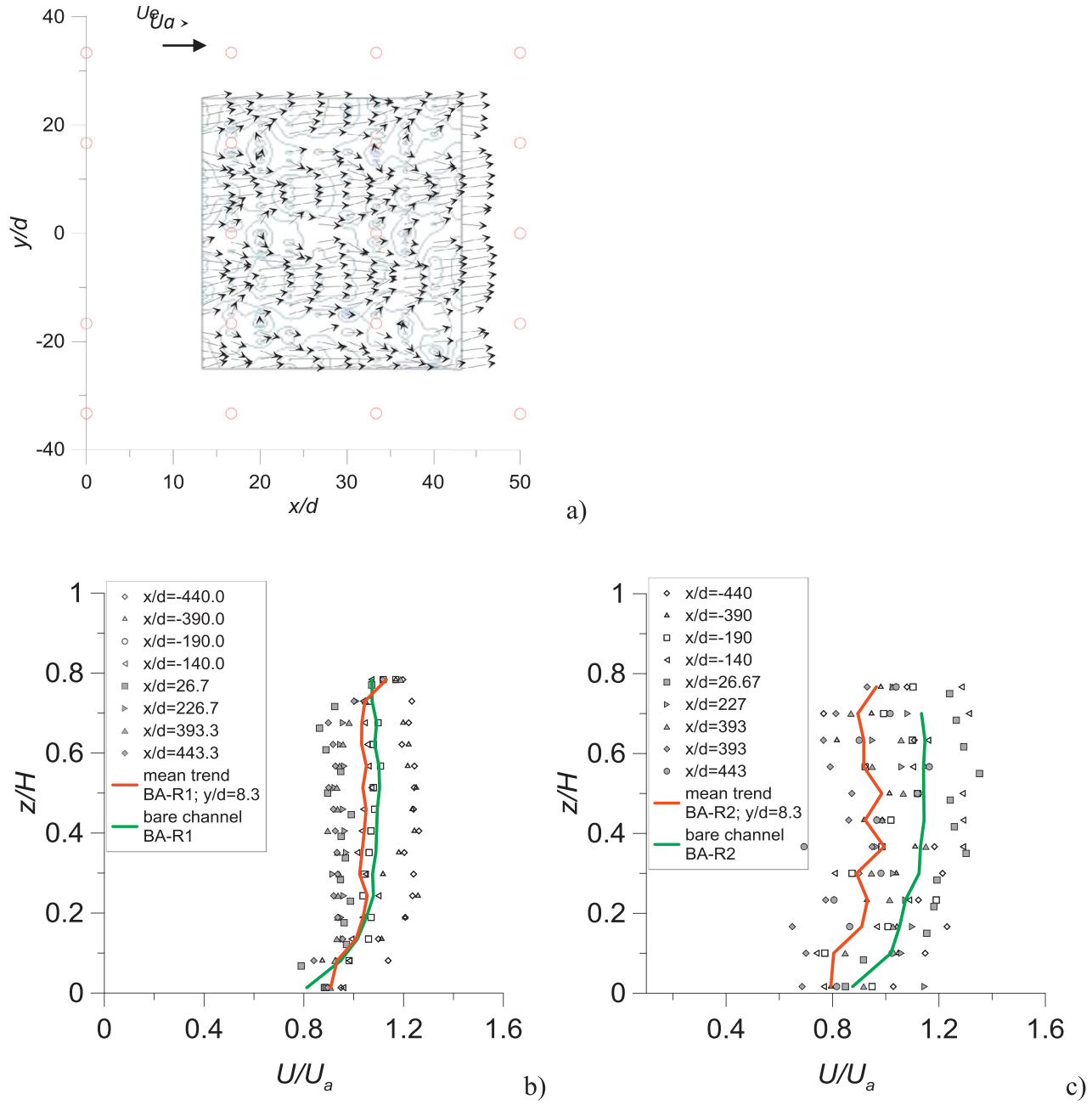

Fig. 3. (a) Horizontal map of the flow velocity distribution in the plane (xy) at $z/H = 0.45$ for the BA-R1 data set; (b) vertical profiles of U/Ua velocity component in the longitudinal section $y/d = 8.3$ at all the investigated x/d positions for the BA-R1 data set and (c) vertical profiles of U/Ua velocity component in the longitudinal section $y/d = 8.3$ at all the investigated x/d positions for the BA-R2 data set. The green line shows the trend for the unobstructed case, while the red line shows the longitudinally averaged profile. (For interpretation of the references to color in this figure legend, the reader is referred to the web version of this article.)

tal run was conducted with water discharge $Q = 35$l/s. The vegetation height H_v (that is the height before producing submergence of vegetation) was about equal to 7.8 cm and the bent vegetation height k_v was about equal to 2.6 cm. The stems concentration was equal to 190 stems/dm^2 at which corresponds a value of the fractional plant area equal to $\phi = 13.5\%$ and $a = 57\text{m}^{-1}$, so that this canopy can be considered dense (Nepf, 2012a, 2012b). The element Reynolds number was $Re_d = 2466$.

During this run the instantaneous longitudinal $u(t)$, transversal $v(t)$ and vertical $w(t)$ velocity components were measured by using the DOP 2000 Profiler by Signal Processing s.a. Three probes of emitting frequency of 8 MHz were used. The DOP2000 allowed the measurement of the instantaneous flow velocity profile along the direction of each probe. Details of the measurement conditions can be found in Termini (2013, 2016a, 2016b).

4. Results

The two experiments are described separately, examining the distributions of the time averaged horizontal velocity, turbulent kinetic energy, integral length scales and diffusivity coefficients. Further, the advective transport of the turbulent kinetic energy due to the mean flow is also investigated. For the sake of simplicity, from now on the time-averaged longitudinal, transversal and vertical velocity components, $\overline{u}$, $\overline{v}$ and $\overline{w}$, will be also referred to as U, V and W, respectively.

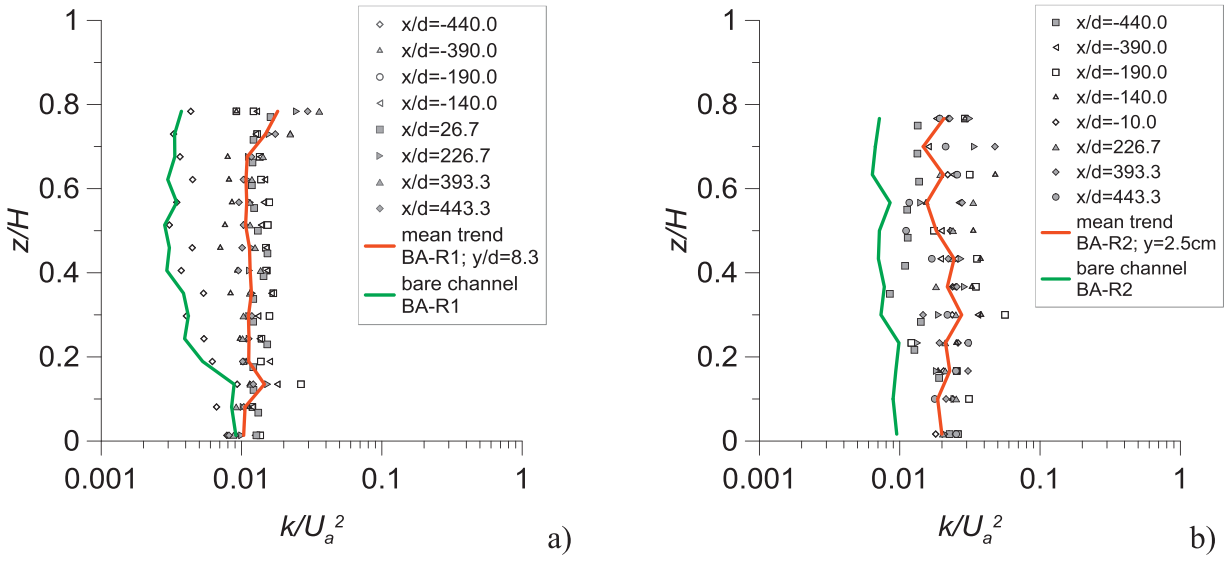

Fig. 4. Vertical profiles of the normalized turbulent kinetic energy in the longitudinal plane $y/d = 8.3$ (a) BA-R1 data set; (b) BA-R2 data set. (For interpretation of the references to color in this figure, the reader is referred to the web version of this article.)

4.1. Results of BA-R data set

For this data set, in run BA-R1values assessed along the longitudinal planes $y = 2.5$ cm (i.e. $y/d = 8.3$) and $y = 0$ (i.e. $y/d = 0$) are available; in run BA-R2 values assessed along the longitudinal planes $y = 2.5$ cm (i.e. $y/d = 8.3$) are available.

As an example, Fig. 3(a) shows in the case of run BA-R1 the typical cylinder effects on the flow velocity distribution in the horizontal plane, computed as $Ut = \sqrt{U^2 + V^2}$, at the intermediate depth $z/H = 0.45$ (for further details, please refer to Ben Meftah and Mossa, 2013; Ben Meftah et al., 2014, 2015). Because of the ADV technical limitations, measurements were not assessed in the uppermost layer, with a thickness of 7 cm. A typical trend is observed in the mapped flow, with the expected behavior of the velocity, showing maxima values in the intermediate position between two consecutive cylinders where the flow converges. Also, the flow diverges from each cylinder, inducing the typical wake. Fig. 3(b) displays for the BA-R1 run the vertical profiles of the time-averaged longitudinal U velocity (normalized by Ua) and plotted for different x/d positions along the longitudinal section at $y/d = 8.3$. The x positions are all located 0.03 m downstream of a cylinder, therefore, in the region of higher velocity. As previously mentioned, the 3D flow is sensitive to the investigated position relative to the stems. In fact, observing Fig. 3(b), we note that the vertical trends of U normalized by Ua are different depending on the relative measuring position x/d with respect to the stems. In any case, to allow a straightforward data comparison, the longitudinal average of the vertical profiles was also considered and plotted on the same graph (red line). This longitudinally-averaged profile of U/Ua was obtained by averaging the data of the different x/d positions at the same z/H. As expected, reduced values of the U/Ua profile are noted in comparison with those of the bare channel (i.e. unobstructed flow), superimposed in Fig. 3(b) (green line). Analogous profiles are shown for the BA-R2 run and $y/d = 8.3$ in Fig. 3(c), where a flattened longitudinally averaged profile of U/Ua is also displayed for the vegetated case in comparison with the unobstructed channel case.

Fig. 4(a) and 4(b) plots the vertical profiles of the time-averaged turbulent kinetic energy, normalized by $U_a{}^2$ for $y/d = 8.3$ of cases BA-R1 and BA-R2, respectively. Also in these graphs, the green and red lines are shown, still referring to the unobstructed flow and to the longitudinally averaged profile of the vegetated flow. In presence of vegetation, increased turbulent kinetic energy values k at all depths and at all x/d positions are evident, if compared to the non-vegetated flow, thus proving the increased turbulent effect induced by the rigid stems on the flow. Moreover, in the unobstructed flow greater values of k are noted near the bed as expected, especially for the BA-R1 run (Fig. 4(a)), with a decreasing trend towards the surface. For the vegetated flow, near the surface, few higher values of normalized k of run BA-R1 are noted, attributable to unavoidable local instabilities.

For the successive key parameters, the analysis is structured in the subsequent way. Firstly, the BA-R1 run is described referring to all values measured at each x/d position along the longitudinal section $y/d = 8.3$. In this way, the local variability of the parameters is evident. Successively, to have a global view, the longitudinally averaged vertical profiles (mean trends) of the vegetated case $y/d = 0$ of the BA-R1 run and $y/d = 8.3$ of BA-R2 run were also added in the graphs. The vertical trends of both BA-R1 and BA-R2 unobstructed cases were also overlaid. In this way, the grouped trends allow a thorough understanding of the dispersion process.

The analysis of Fig. 5 shows the integral turbulent lengths, normalized by d, along the three directions, i.e. lx, ly and lz, calculated by means of Eq. (11), referring to all points investigated in BA-R1 run, in the longitudinal plane $y/d = 8.3$. As previously written, in the case of the unobstructed channel, the integral length scale of turbulence l is of order of the channel flow depth H. Instead, the presence of the array, its density and arrangement of the plants, modify the structure of the turbulent flow (Righetti, 2008). In fact, it is worth noting that, for the bare channel flow, the values of lx are of the same order of magnitude of the channel height, i.e. $O(10^{-1})$, consistently with Okubo (1971) Nepf (1999). The presence of the vegetation induces a reduction of lx, which is characterized by a lower order of magnitude in comparison with the unobstructed case, i.e. $O(10^{-2})$ and comparable with the canopy pore s. On the contrary, in the transversal direction, the length ly increases when vegetation is present, in comparison with the non-vegetated case, even if the order of magnitude of ly is $O(10^{-4})$ for both unobstructed and obstructed cases. The turbulent length lz in the vertical direction is reduced in the obstructed flow in comparison with the unobstructed case, keeping the same order of magnitude $O(10^{-4})$. The behavior observed in Fig. 5 highlights that the turbulent eddies are affected by the symmetrical and equally spaced

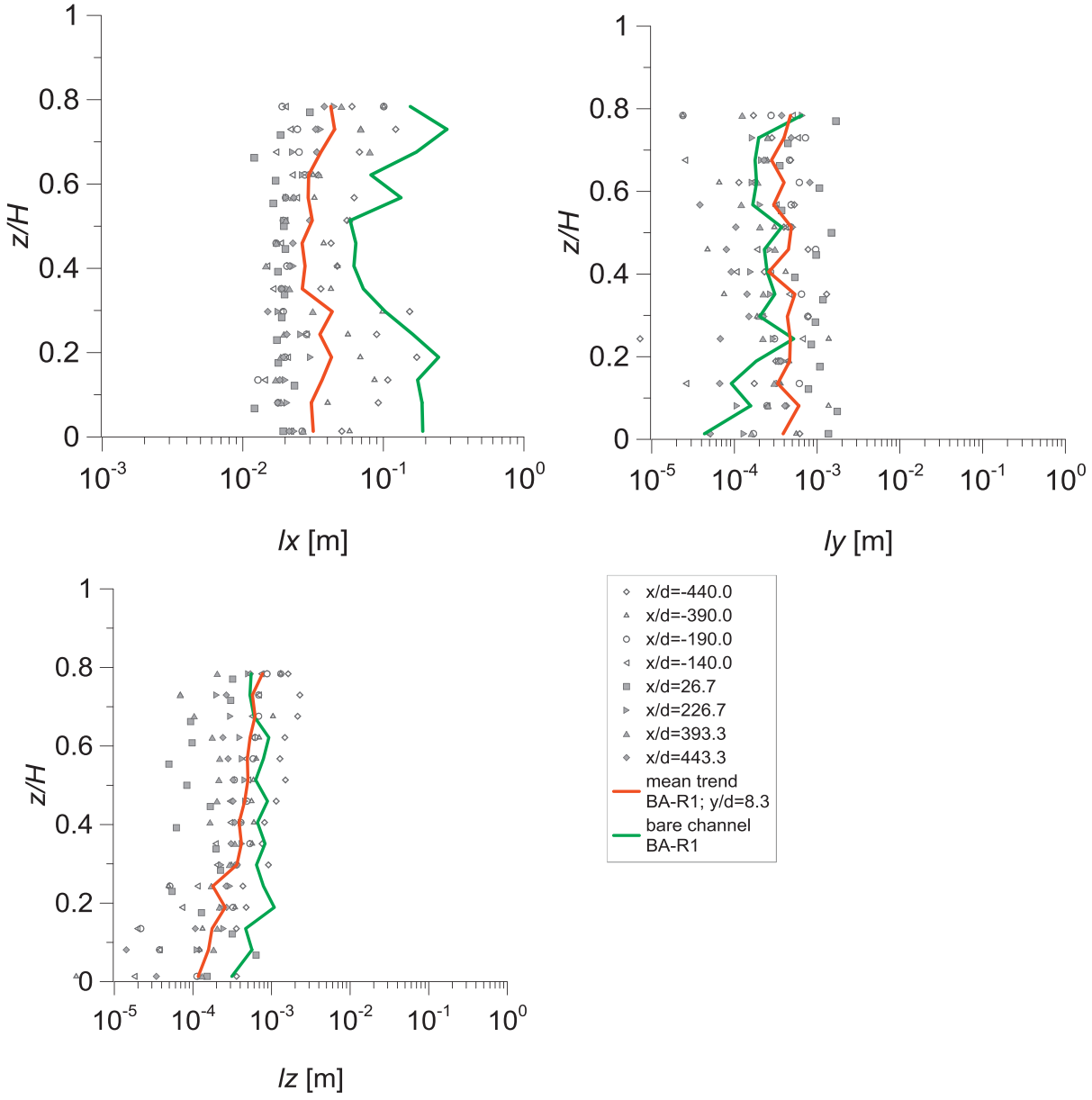

Fig. 5. Vertical profiles of the integral length scales *lx*, *ly* and *lz*, in the longitudinal section $y/d = 8.3$. BA-R1 data set.

rigid stems, thus becoming flattened in the longitudinal and vertical directions while they stretch in the transversal one.

For *lx*, *ly* and *lz*, Fig. 6 collects the vertical profiles of the unobstructed flow of BA-R1 and BA-R2, as well as the longitudinally averaged vertical profiles (mean trends) of BA-R1 for $y/d = 0$ and $y/d = 8.3$ and of BA-R2 for $y/d = 8.3$. Three different logarithmic abscissa axes are inserted, to identify if the turbulent length scale is scaled by *d*, *s* or *H* (considering that *H* is different for BA-R1 and BA-R2 runs, the reference value $H = 0.3$ m was used).

Namely, the analysis of *lx* (Fig. 6) is interesting and marks the novelty of the present research. In fact, as previously written, in the present case of sparse vegetation with $ad < O(0.01)$, it was expected that the integral length scale of turbulence was of $O(d)$, consistently with Nepf et al. (1997) and Lopez and Garcia (1998). Fig. 6 confirms that when vegetation is absent (bare channel BA-R1 and bare channel BA-R2) *lx* has the order of magnitude of *H*. In addition, it reveals that when $y/d = 8.3$, *lx* has the order of magnitude of *s*; while when $y/d = 0$, *lx* has the order of magnitude of *d*. Therefore, for this sparse rigid vegetation a heterogeneous and locally variable behavior of *lx* is verified. It depends not only on the density of the canopy but also on the position relative to the stems. For both runs BA-R1 and BA-R2, in the longitudinal plane $y/d = 8.3$ where in-line stems are absent (Fig. 1), turbulent eddies tend to occupy all the available stem-to-stem distance and *lx* is scaled by *s*, which on the contrary should occur when $d > s$, according to previous research. In contrast, for the longitudinal plane $y/d = 0$ (BA-R1 run) where in-line stems are present (Fig. 1), turbulent eddies are in the stem wake and blocked by the same stems, so that the canopy behaves as expected, with *lx* scaled by *d*.

Fig. 6 displays the mean trends of *ly*, assembled for all the investigated cases, and illustrates that *ly* is increased by approximately one order of magnitude by the presence of the stems. The mean trends of *lz* are also shown in the same figure, where the presence of the stems induces a reduction of about one order of magnitude, specifically in the BA-R1 case for $y/d = 0$.

For the BA-R1 run and $y/d = 8.3$ the vertical profiles of the dispersion coefficients *Kxx*, *Kyy* and *Kzz*, computed with Eq. (12) and using $\alpha = 0.9$, are plotted in Fig. 7, normalized by $U_a d$. The coef-

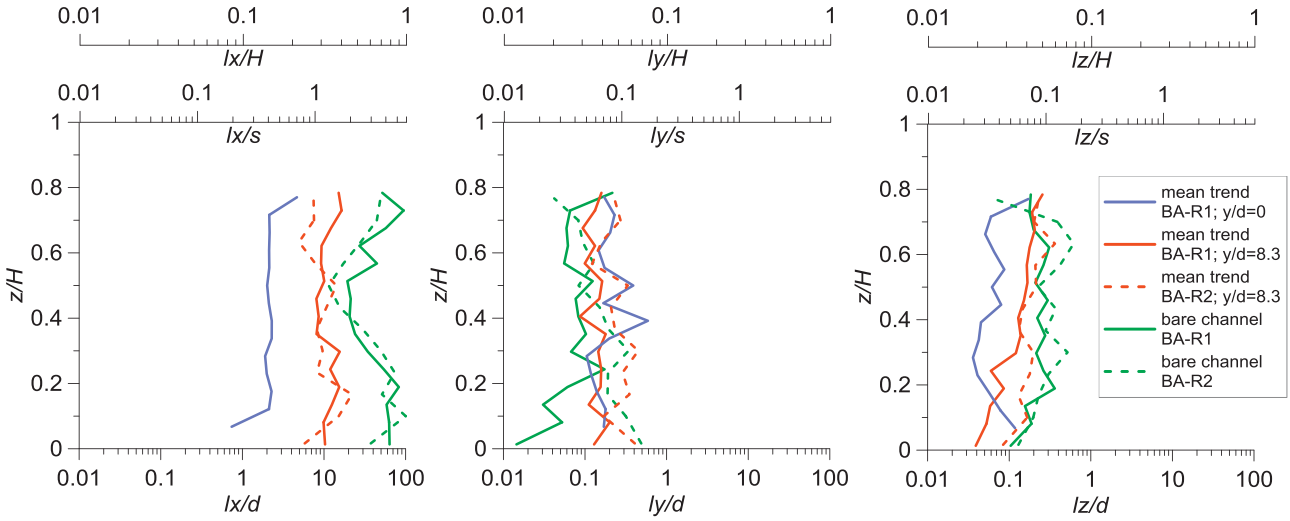

Fig. 6. Mean vertical profiles of the integral length scales *lx*, *ly* and *lz*, for all the assessed data.

ficients *Kxx* and *Kyy* display trends resembling those of the corresponding turbulent lengths. In fact, in the longitudinal direction, the dispersion coefficients are reduced by the presence of vegetation, while they increase in the transversal direction. Referring to *Kzz*, the two vertical profiles, of the unobstructed flow and of the vegetated flow longitudinally averaged, show analogous trends.

The global view of the dimensionless dispersion coefficients is shown in Fig. 8, where all the mean trends are assembled for a meaningful assessment. The above described trends are confirmed. Specifically, the values of *Kxx* for the BA-R1 run and $y/d = 0$ are around two order of magnitudes lower than in the case of the bare channel and one order of magnitude lower than in the cases $y/d = 8.3$ of runs BA-R1 and BA-R2. The transversal dispersion coefficients *Kyy* increase of one order of magnitude when vegetation is present for both cases BA-R1 and BA-R2. The vertical dispersion coefficients are much smaller than the longitudinal and transversal dispersion coefficients. Furthermore, they are smaller in the obstructed cases, especially in the layers closer to the bottom and the surface.

Fig. 9 displays for the BA-R1 run and $y/d = 8.3$ the advective transport of k by the time-averaged flow in the longitudinal, transversal and vertical direction, normalized by $U_a{}^3$. The advection towards the transversal and vertical directions is quite nil, for both cases of obstructed and unobstructed flows, as shown by the average trends.

On the contrary, the longitudinal advection in the vegetated flows is greater than that of the same flows without vegetation, thus proving that in the vegetated runs the increase of the k values prevails on the reduction of the time-averaged velocity in the product *Uk*. The global trend of Fig. 10 confirms this observation. Furtherly, the same figure highlights that the increase of the longitudinal advection is mainly evident in the BA-R2 run, where Re_d is greater than in the run BA-R1.

4.2. Results of PA-F data set

Fig. 11(a) shows the horizontal distribution of the resultant horizontal velocity $Ut = \sqrt{U^2 + V^2}$ at $z/H = 0.42$ along a stretch of the vegetated-bed (run PA-F). In this figure the formation of alternating zones of high/low values of flow velocity can be seen. Fig. 11(b) shows the vertical profiles of the averaged longitudinal U velocity, normalized by *Ua*, for different x/d positions: $x/d = 133.3$ (i.e. at a distance of 40 cm from the initial section $x = 0$), $x/d = 266.6$ (i.e. at a distance of 80 cm from the initial section $x = 0$), $x/d = 400.0$ (i.e. at a distance of 120 cm from the initial section $x = 0$). The corresponding averaged profile (red line) is compared with the vertical profile (green line) obtained at position $x/d = 666.6$ (i.e. at section distant 200 cm from the initial section) without vegetation on the bed. Unlike in the case where there is an absence of vegetation, in the presence of vegetation the velocity profile shows the typical S-shape. In fact, the presence of dense vegetation generates a region of shear and a profile with an inflection point near the top of the canopy (see also Nepf, 2012a, 2012b; Carollo et al., 2005; Termini, 2015, 2016a).

Fig. 12 shows the vertical profiles of the turbulent kinetic energy, normalized by the square of the mean flow velocity U_a^2, estimated at different locations along the channel axis. In this figure the profiles of the spatial average of turbulent kinetic energy and of the turbulent kinetic energy estimated at the position $x/d = 700.0$ (i.e. at section distant 210 cm from the initial section, without vegetation on the bed) both normalized by the square of the mean flow velocity U_a^2, are also reported.

This figure shows that in presence of vegetation the value of the turbulent kinetic energy increases inside the vegetated layer. It reaches a peak value at a relative water depth approximately equal to $z/H = k_v/H = 0.24$ and it decreases towards the free surface. Thus, according to Nepf and Vivoni (2000), k/U_a^2 increases in the shear region. At the position $x/d = 700.0$ (without vegetation on the bed) the turbulent kinetic energy shows a decreasing trend from the bed towards the free surface, as observed in the case of unobstructed flow for the BA-R data set. In the absence of vegetation, k/U_a^2 assumes values greater than those obtained in the upstream positions with vegetation on the bed. This could be due to the fact that the presence of dense vegetation offers additional resistance determining flow velocity always less than that over conditions without vegetation (bare bed) (see also Nepf, 1999, 2012a).

Fig. 13 shows the integral turbulent lengths, normalized by d, along the directions *x, y, z*, estimated for the PA-F run. In this case, the order of magnitude of the integral scale *lx* remains almost invariant, i.e. O(d), even if a reduction is observed in the obstructed case. Similar behavior is also noted in the vertical and transversal directions, for the integral scales *ly* and *lz*. This is consistent with results obtained by Tanino and Nepf (2008) in random cylinder arrays with $\phi = 0.01 \div 0.35$. It is noteworthy that in the case of the dense canopy the behavior for the turbulent length scales is nearly isotropic.

The vertical profiles of the dispersion coefficients *Kxx, Kyy* and *Kzz*, normalized by $U_a d$, are plotted in Fig. 14. In this case, all the

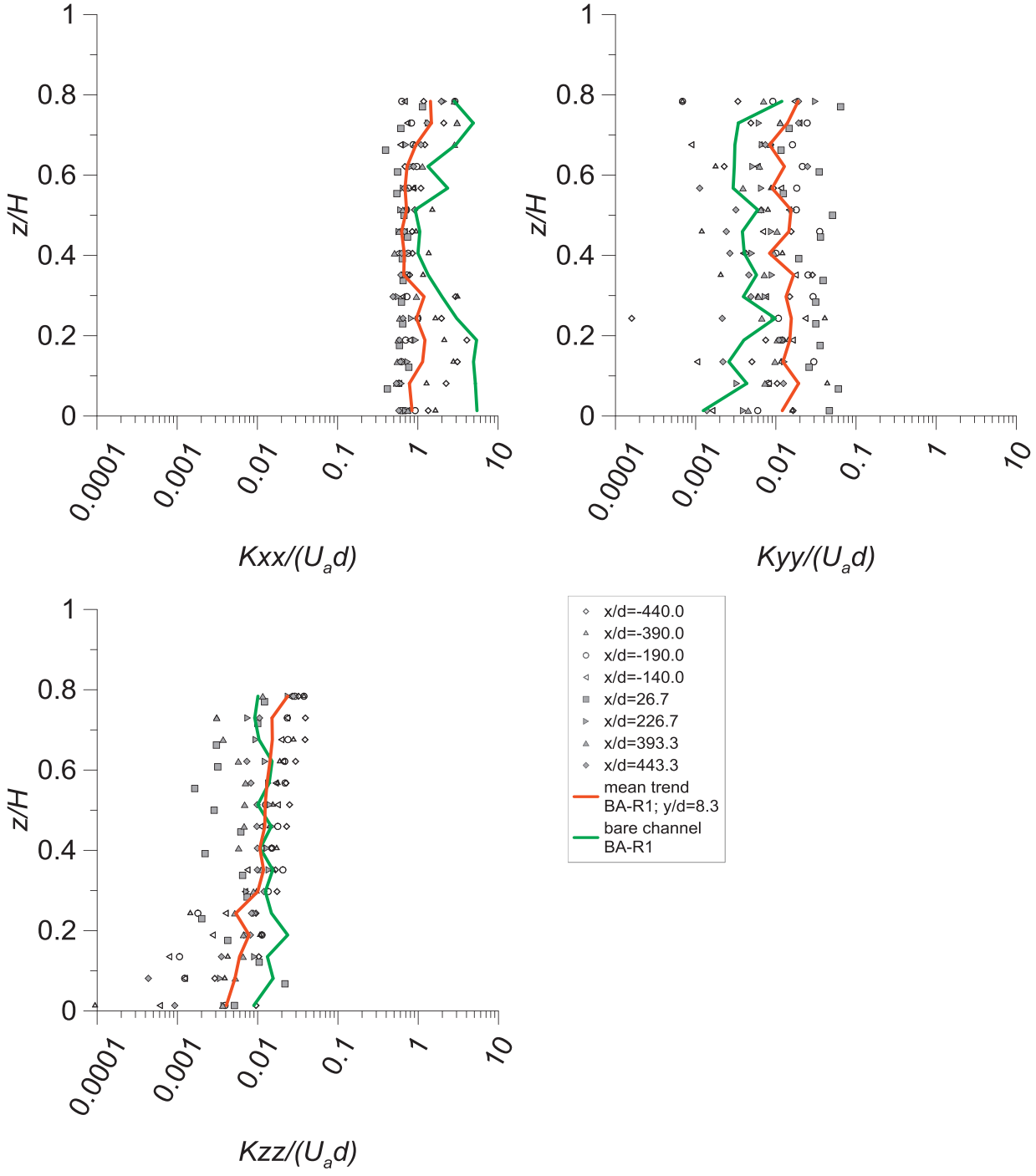

Fig. 7. Vertical profiles of the normalized dispersion coefficients *Kxx, Kyy* and *Kzz*, in the longitudinal plane $y/d = 8.3$. BA-R1 data set.

dispersion coefficients (*Kxx, Kyy, Kyy*) assume in presence of vegetation values lower than those obtained in absence of vegetation. This is particularly evident in the longitudinal direction.

The advective transport of k by the time-averaged flow, normalized by $U_a{}^3$, is displayed in Fig. 15. When vegetation is present, the spatially averaged transport in the transversal and vertical directions is around zero, while it assumes positive values in the unobstructed flow. In the longitudinal direction, the spatially averaged advective transport in presence of vegetation is reduced with respect to the unobstructed case. In both cases the spatially averaged advective transport shows an increasing trend from the bed towards the free surface, increasing in the shear region and reaching a maximum value at $z/H \cong 0.4$; then it decreases again.

5. Discussion

A reasonable analysis of the two examined data sets, which are characterized by very different canopies, rigid emergent and flexible submerged respectively, can be carried out only if we take in due count that: (i) the value of Re_d characterizing the PA-F data set is about 5 times greater than the corresponding one of the BA-R data set, (ii) the vegetation density a characterizing the PA-F data

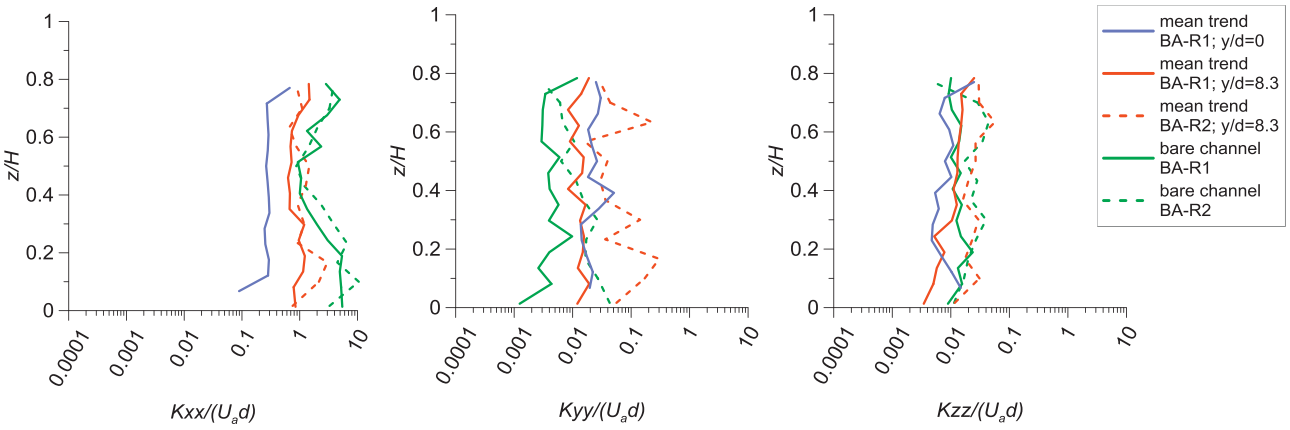

Fig. 8. Mean trend of the vertical profiles of the dispersion coefficients for all the assessed data.

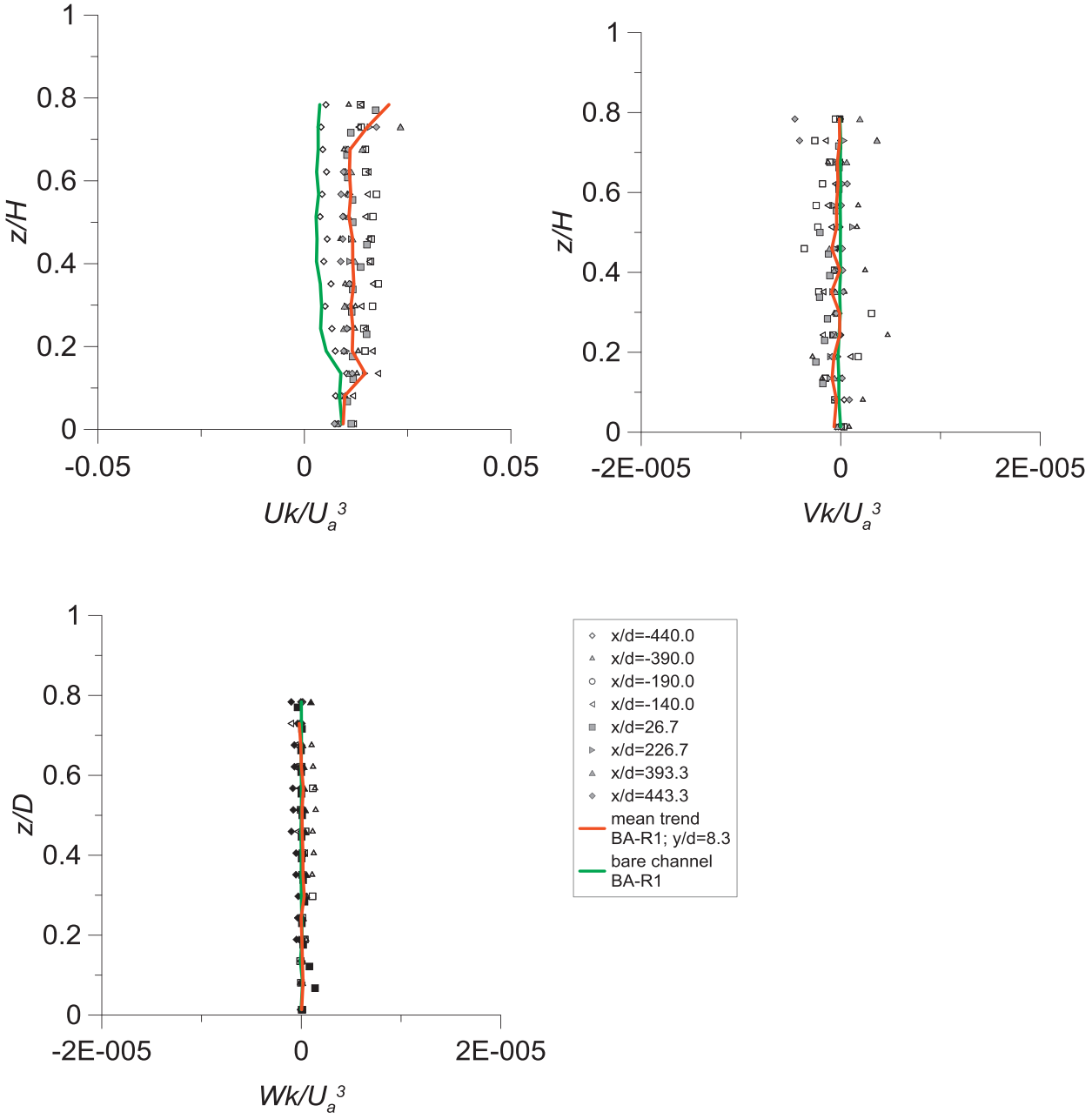

Fig. 9. Vertical profiles of the longitudinal, transversal and vertical advective transport of turbulent kinetic energy by the time-averaged flow, in the longitudinal plane $y/d = 8.3$. BA-R1 data set.

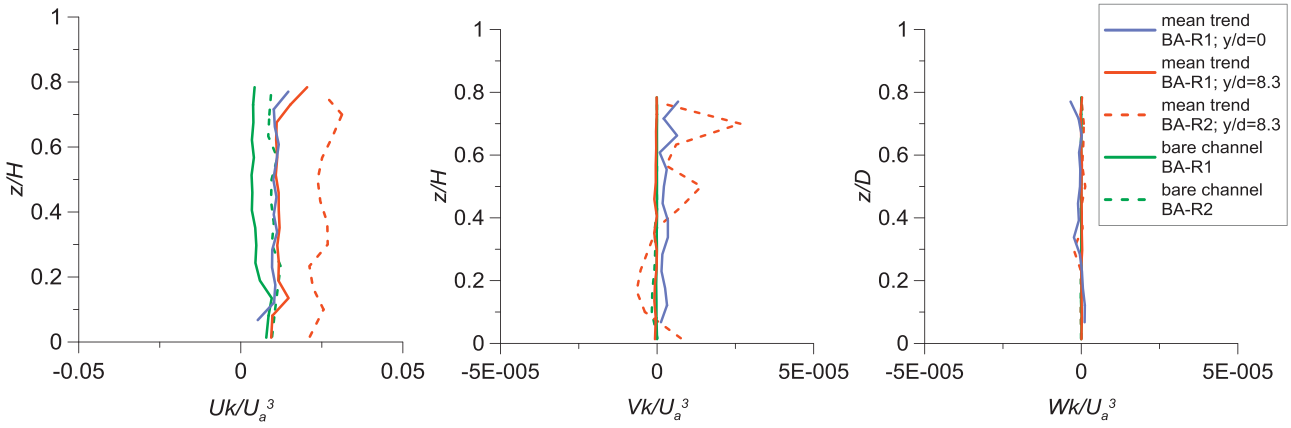

Fig. 10. Mean trend of vertical profiles of the longitudinal, transversal and vertical advective transport of turbulent kinetic energy by the time-averaged flow for all the assessed data.

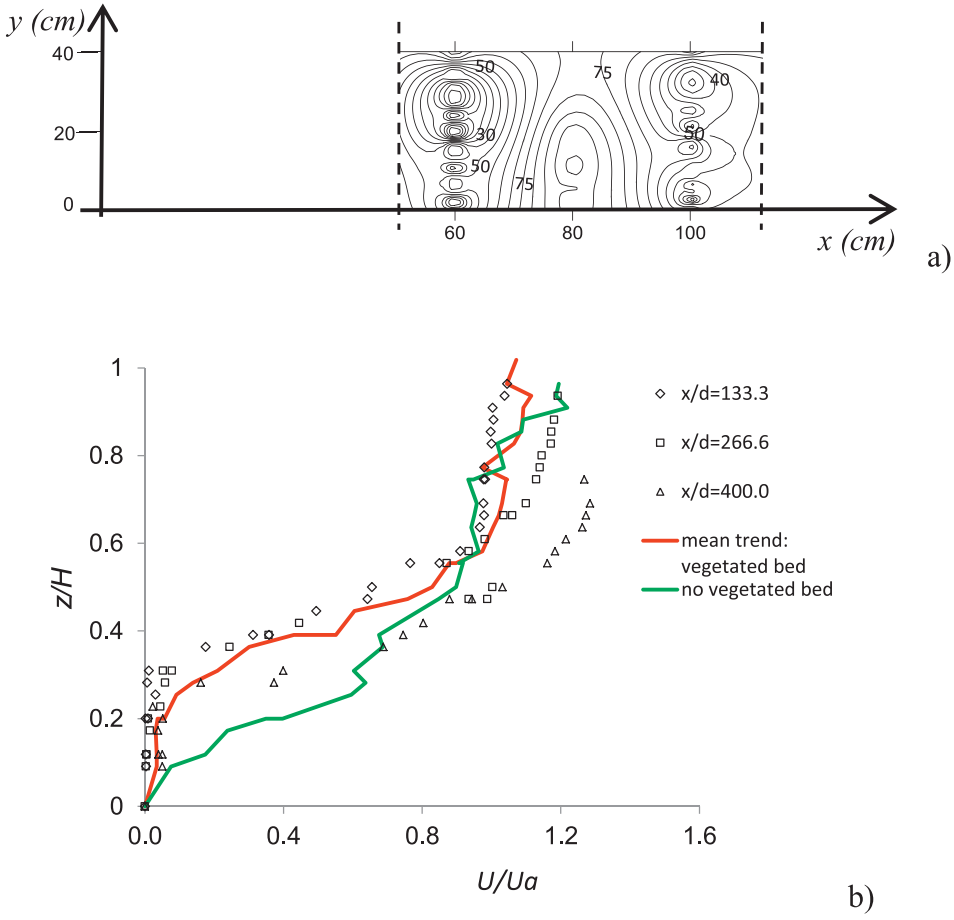

Fig. 11. (a) Horizontal map of the flow velocity U_t (cm/s) distribution in the plane (xy) at $z/H = 0.42$ along the vegetated-bed reach for PA-F data set; (b) vertical profiles of U/Ua velocity component. PA-F data set. (For interpretation of the references to color in this figure, the reader is referred to the web version of this article.)

set is about 50 times greater than the corresponding one of the BA-R data set.

Therefore, in this research, the role played by both stem Reynolds number and canopy density in the mechanism of dispersion and transport was examined in-depth, being not entirely understood. In fact, White and Nepf (2003) suggested that longitudinal dispersion due to vortex trapping may change with density. At the same time, vortex trapping is also heavily influenced by terms dependent on Re_d, which remains the same between densities. Sonnenwald et al. (2017) deduced that transverse dispersion data does not suggest a dependency on solid volume fraction, whereas there is some indication of an inverse trend between longitudinal dispersion and solid volume fraction. Guo et al. (2014) in their numerical model for periodic arrays of cylinders showed that longitudinal and transverse dispersion increased with decreasing solid volume fraction in a diamond array of vegetation.

To examine how our experimental results are affected by Re_d and vegetation density, we firstly analyzed the distribution of the turbulent kinetic energy k. In the unobstructed case, for both PA-F and BA-R data sets, a decreasing trend is noted from the bot-

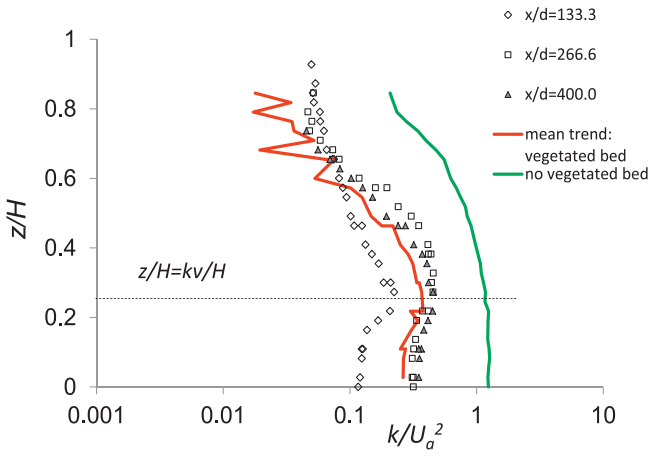

Fig. 12. Vertical profiles of the normalized turbulent kinetic energy. PA-F data set.

tom, where turbulence is high because of the bed roughness, towards the surface. The vertical gradient of k is greater for the PA-F than for the BA-R observations. On the contrary, when vegetation is present, the behavior in the two data sets is different. In fact, the low density of the rigid vegetation BA-R allows the flow to move inside the patch and the obstructive mechanism increases the turbulent kinetic energy compared to the non-vegetated flow (Fig. 4) as also noted in the experiments by Maji et al. (2016). On the contrary, in the PA-F data set (Fig. 12) the presence of the vegetation reduces the turbulent kinetic energy with respect to the non-vegetated flow, because the densely distributed flexible stems act as a blockage, inducing an increased drag and a reduction of the mean flow U. This is consistent with results obtained by Nepf (1999, 2012a, 2012b) by comparing flow velocity and kinetic energy profiles for different densities of canopy including the bare bed condition. It is also worth noting that in the BA-R experiments the observations are sensitive to the relative position of the measuring point with respect to the stems.

The analysis of the integral length scales leads to the following deductions. As previously mentioned, the unobstructed flow of the BA-R case shows values of lx of order of O(H), while in the obstructed flow lx assumes order O(d) or O(s) depending on the measuring position relatively to the stems (Fig. 6). This result is novel as compared with previous studies (Nepf, 1997, 1999; Shivpure et al., 2016). Namely, in the wake region it is O(d) while between stems it is O(s). It is worth noting that, vortex trapping and stem-scale secondary wake dispersion are primarily responsible of longitudinal dispersion in emergent vegetation (White and Nepf, 2003). In vortex trapping, particles are entrained temporarily in the eddies formed behind stems, while in secondary wake dispersion, particles travel between areas of lower velocity behind stems and higher velocity between stems. Our result on lx proves the presence of this differential longitudinal advection. For the vegetated case, even the reduction of lz is noted. While lx and lz values reduce, values of the transversal ly increase, thus expecting turbulent eddies flattened in the longitudinal and vertical direction but transversally stretched, with respect to the unobstructed flow. This behavior reveals the anisotropy of turbulence spreading in the case of sparse vegetation. This conclusion is noteworthy, since the spatial average technique, generally used in literature, prevents any 3D analysis.

In the PA-F experiment the lx, ly and lz are always reduced in the obstructed flow, with order of magnitudes comparable to d (Fig. 13). Therefore, in the dense canopy, turbulence is characterized by isotropy. This result further demonstrates that dense vegetation intercepts and blocks the turbulent eddies, independently

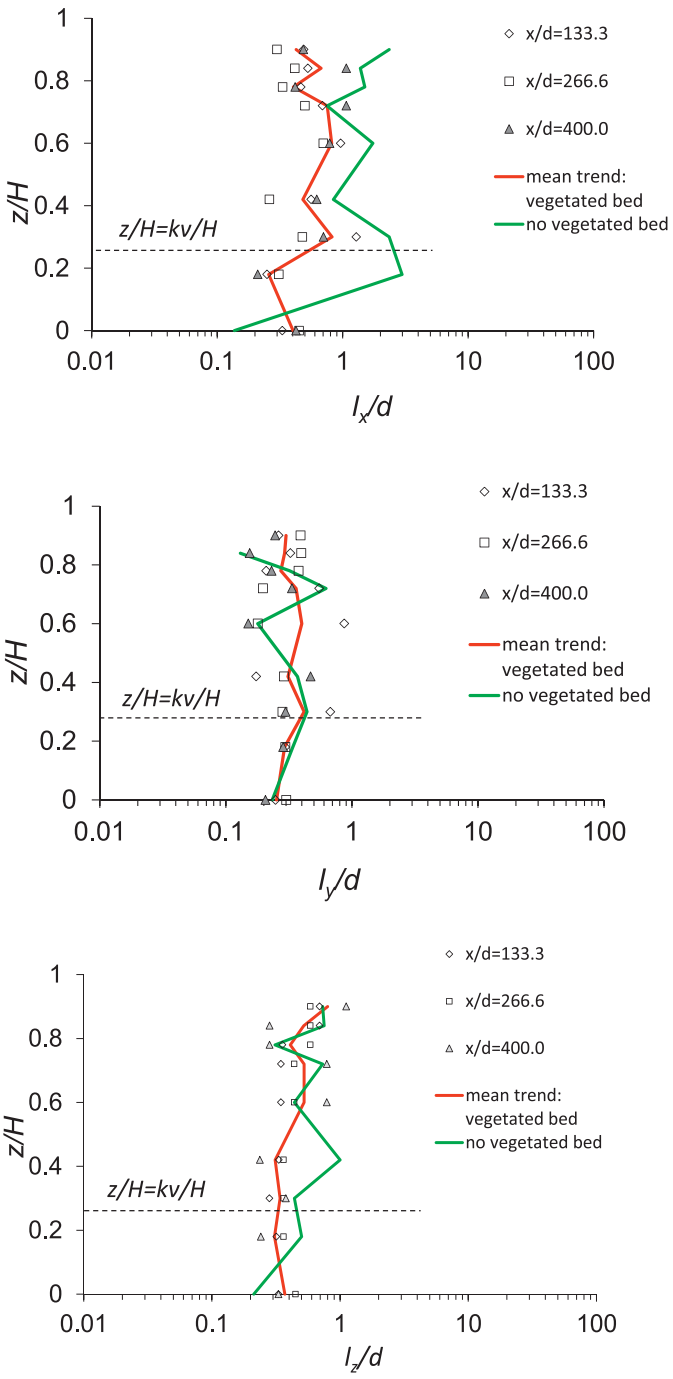

Fig. 13. Vertical profiles of the integral length scales lx, ly and lz, in the longitudinal plane $y = 0.20$ m. PA-F data set.

on the direction, especially due to the overlapping of stem wakes. On the contrary, rigid and sparse vegetation allows a transversal spreading of turbulent patterns, thus making the transversal direction a favorite path for turbulent eddies.

The dispersion coefficients of the BA-R data set show vertical trends like those of the integral length scales (Figs. 7 and 8). The reduction of the dispersion coefficients in the longitudinal direction due to vegetation is confirmed. Namely, this reduction is one order of magnitude greater for the position $y/d = 0$ with respect to the position $y/d = 8.3$, thus proving the influence of the relative position of the stems on the measurement points. Further, considering Eq. (12) used for the computation of Kjj coefficients, it should

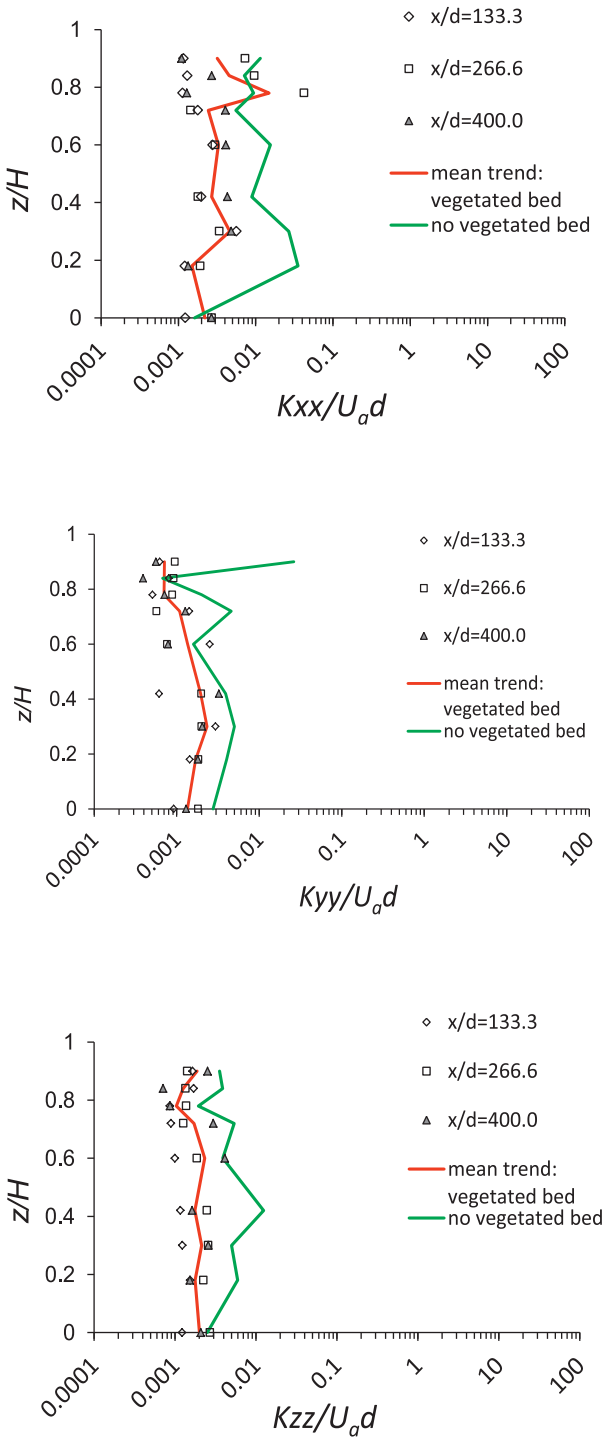

Fig. 14. Vertical profiles of the normalized dispersion coefficients *Kxx, Kyy* and *Kzz*. PA-F data set.

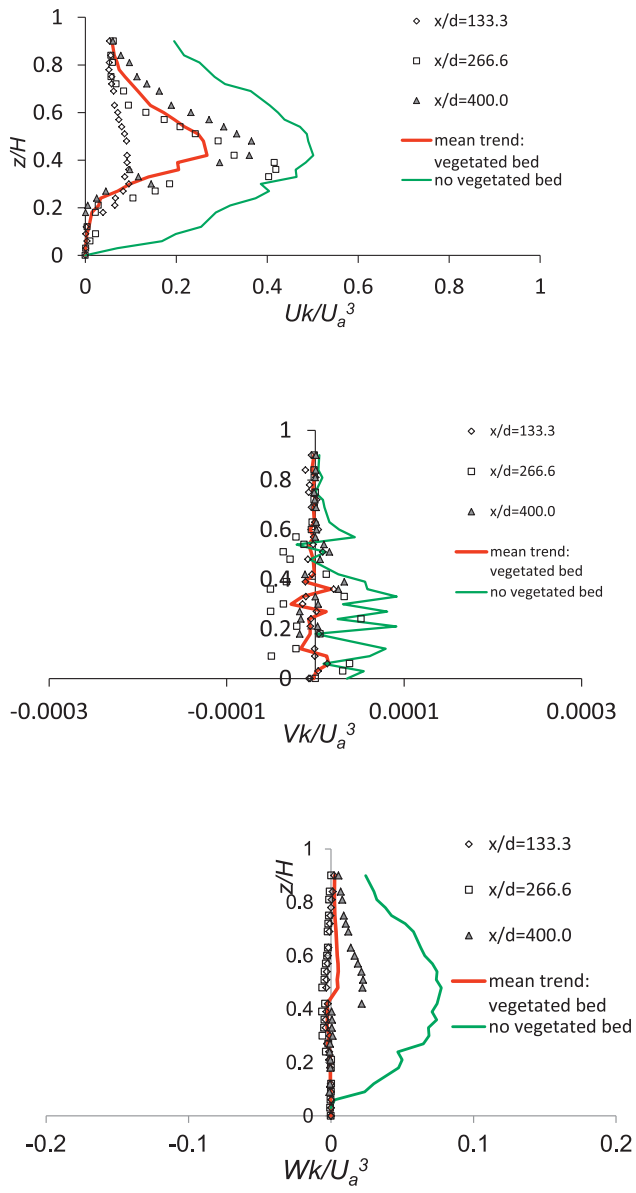

Fig. 15. Vertical profiles of the normalized longitudinal, transversal and vertical advective transport of turbulent kinetic energy (by the time-averaged flow). PA-F data set.

be noted that in the vegetated case the reduction of *lx* prevails on the increase of $\sqrt{k}$, thus providing reduced *Kxx* values. On the contrary, the transversal dispersion coefficients *Kyy* increase of one order of magnitude in the vegetated flow. This increase is more evident for run BA-R2 than for run BA-R1, thus showing that Re_d is a key parameter in this transversal turbulent process. The vertical dispersion is negligible if compared to the longitudinal and transversal ones.

The examined dispersion mechanism is consistent with the sparse location and the pattern of the rigid canopy, frontally impeding the development of the turbulent eddies, but allowing their development transversally on both sides. The transversal dispersion is even greater when the Re_d number is greater. The anisotropy of turbulence is proved again, as well as the presence of secondary currents, which advect turbulence spanwisely, confirming also results by Nezu and Onitsuka (2001).

The longitudinal advective transport of *k* in the BA-R experiment was expected to be lower in the vegetated flow than in the unobstructed one. On the contrary, it results greater for the vegetated case (Figs. 9 and 10). This could be explained considering that in the vegetated flow, two competing effects are present, i.e. reduced velocity and increased turbulence (Nepf, 2012a, 2012b). These opposing tendencies are responsible for an initial increasing of turbulence due to the presence of sparse stems, as in the BA-R case (Fig. 4), but eventually turbulence decreases when the vegetation density increases further, as in the PA-F case (Fig. 12). In fact, the behavior within the flexible stems of the PA-data set shows turbulent eddies smaller in size (Fig. 13), with a consequent

reduction of the dispersion coefficients along all three directions (Fig. 14). The flexible and dense system behaves as a 'filter' which determines a reduction of the turbulent flow features and prevents high rates of the advective transport of k (Fig. 15). This is reliable with previous results in literature (see as an example Nepf, 2012a, 2012b) demonstrating that, at stem scale, the length scale of the developing vortices is set by the stem diameter, and this length scale partially controls the characteristic eddy size which develops within and between the vegetated elements (Termini, 2016b, 2017).

Therefore, consistently with Eqs. (4) and (9), applying the analogy between the transport of TKE and the transport of a solute/tracer, it can be highlighted that the transport of a scalar in a canopy is heterogeneous and spatially variable and is strictly governed by the density of the canopy. In fact, for high values of vegetation density, the transport and dispersion of a tracer is strongly inhibited along all the three directions. In the case of sparse vegetation, a transversal path is permitted to turbulent eddies, depending on both canopy density and stem Reynolds number, while the advective longitudinal transport depends on the relative prevalence of channel velocity or turbulence. It could be argued that even suspended sediments could experience an analogous mechanism of spreading.

6. Concluding remarks

Experiments with vegetated channels were executed in the case of both flexible submerged and rigid emergent canopies. Specifically, the process of transport and dispersion of tracers was investigated, once noted that it resembles the transport and dispersion of turbulent kinetic energy k.

The principal findings are summarized below.

In presence of vegetation, for both canopy configurations a reduction of the mean longitudinal velocity is experienced. On the contrary, vegetation differently affects the two configurations, referring to k. The sparse and rigid vegetation of the BA-R runs induces an increasing of turbulent kinetic energy, while in the PA-F data set the dense and flexible stems reduce k, acting as a filter.

With reference to the integral length scales, in the sparse canopy (BA-R) the longitudinal turbulent scale lx of the unobstructed channel is of O(H), while it is reduced by the presence of the stems and scaled by d or s, according to the measuring position relatively to the stems. Namely, in the wake region it is O(d) while between stems it is O(s). This heterogenous behavior, locally variable and dependent on the position, consistent with vortex trapping and wake dispersion, is a novel outcome with reference to previous researches. The vertical length scale lz is reduced, while the transversal length scale ly is increased by the presence of the stems, thus expecting turbulent eddies flattened in the longitudinal and vertical direction but transversally stretched, compared to the unobstructed flow. This behavior reveals the anisotropy of turbulence spreading in the case of sparse vegetation.

In the dense canopy (PA-F) the lx, ly and lz turbulent scales are always reduced in presence of vegetation, with order of magnitudes even smaller than d. As an interesting result, in the dense canopy, turbulence is characterized by isotropy.

The trends for the dispersion coefficients follow those of the turbulent scales. In fact, in presence of vegetation, they are reduced along the three directions in the PA-F data set, while in the BA-R data set a reduction is noted only for the longitudinal and vertical ones. The transversal dispersion coefficients increase with the stem Reynolds number.

The analysis of the experimental results highlights that the density of the canopy is the key parameter in the advective processes. In fact, the transport of k and therefore of a possible solute is strictly dependent on the density of the canopy. Only for high values of vegetation density, the transport and dispersion of a tracer is obstructed along all directions. In the case of sparse vegetation, turbulent eddies and tracer transport have a favorite transversal path, regulated by both canopy density and stem Reynolds number. In the longitudinal direction, the advective transport depends on the relative prevalence of channel velocity or turbulence.

References

Ben Meftah, M., Mossa, M., 2013. Prediction of channel flow characteristics through square arrays of emergent cylinders. Phys. Fluids 25 (4), 1–21.

Ben Meftah, M., De Serio, F., Mossa, M., 2014. Hydrodynamic behavior in the outer shear layer of partly obstructed open channels. Phys. Fluids 26 (6), 1–19.

Ben Meftah, M., De Serio, F., Malcangio, D., Mossa, M., Petrillo, A.F., 2015. Experimental study of a vertical jet in a vegetated crossflow. J. Environ. Manag. 9.

Ben Meftah, M., Mossa, M., 2016. Partially obstructed channel: contraction ratio effect on the flow hydrodynamic structure and prediction of the transversal mean velocity profile. J. Hydrol. 542.

Ben Meftah, M., De Serio, F., Malcangio, D., Mossa, M., 2017. Vertical dense jet in flowing current. Environ. Fluid Mech. 17, 1–22.

Carollo, F.G., Ferro, V., Termini, D., 2005. Flow Resistance law in channels with flexible submerged vegetation. J. Hydraul. Eng 131, 554–564.

Costanza, R., D'Arge, R., De Groot, R., Farber, S., Grasso, M., Hannon, B., Limburg, K., Naeem, S., Oneill, R.V., Paruel, J., Raskin, R.G., Sutton, P., van den Belt, M., 1997. The value of the world's ecosystem services and natural capital. Nature 387, 253–260.

Crosato, A., Saleh, M.S., 2011. Numerical study on the effects of floodplain vegetation on river planform style. Earth Surf. Process. Landf. 36, 711–720.

Cuthbertson, A.J.S., Malcangio, D., Davies, P.A., Mossa, M., 2006. The influence of a localised region of turbulence on the structural development of a turbulent, round, buoyant jet. Fluid Dyn. Res. 38, 683–698.

De Serio, F, Mossa, M, 2014. Streamwise velocity profiles in coastal currents. Environ. Fluid Mech. 14, 895–918.

De Serio, F, Mossa, M, 2015. Analysis of mean velocity and turbulence measurements with ADCPs. Adv. Water Res. 81, 172–185.

Finnigan, J.J., 1985. Turbulent transport in flexible plant canopies. In: Hutchison, B.A., Hicks, B.B. (Eds.), The Forest-Atmosphere Interaction. Reidel Publishing Company, pp. 443–480.

Ghisalberti, M., Nepf, H., 2004. The limited growth of vegetated shear layers. Water. Resour. Res. 40, W07502.

Ghisalberti, M., Nepf, H., 2005. Mass transfer in vegetated shear flows. Environ. Fluid Mech. 5 (6), 527–551.

Ghisalberti, M., Nepf, H., 2006. The structure of the shear layer over rigid and flexible canopies. Environ. Fluid Mech. 6 (3), 277–301.

Ghisalberti, M., Nepf, H., 2009. Shallow flows over a permeable medium: the hydrodynamics of submerged aquatic canopies. Transp. Porous Media 78 (2), 309–326.

Gregory, S.V., Swanson, F.J., McKee, W.A., Cummins, K.W., 1991. An ecosystem perspective of riparian areas. BioScience 41, 540–551.

Guo, X., Wang, B., Mei, C.C., 2014. Flow and solute transport through a periodic array of vertical cylinders in shallow water. J. Fluid Mech. 756, 903–934.

Gurnell, A., 2014. Plants as river system engineers. Earth Surf. Process. Landf. 39 (1), 4–25.

Ikeda, S., Kanazawa, M., 1996. Three-Dimensional organized vortices above flexible water plants. J. Hydraul. Eng. 122 (11).

Kemp, J.L., Harper, D.M., Crosa, G.A., 2000. The habitat-scale eco-hydraulics of rivers. Ecol. Eng 16 (1), 17–29.

Lima, A.C., Izumi, N., 2014. Linear stability analysis of open-channel shear flow generated by vegetation. J. Hydraul. Eng. 140, 231–240.

Liu, C., Nepf, H., 2016. Sediment deposition within and around a finite patch of model vegetation over a range of channel velocity. Water Resour. Res 52, 600–612.

López, F., García, M., 1998. Open-channel flow through simulated vegetation: suspended sediment transport modeling. Water Resour. Res. 34, 2341–2352.

Lotsari, E., Thorndycraft, V., Alho, P., 2015. Prospects and challenges of simulating river channel response to future climate change. Progress in Physical Geography 39 (4), 1–31.

Maji, S., Pal, D., Hanmaiahgari, P.R., Pu, J.H., 2016. Phenomenological features of turbulent hydrodynamics in sparsely vegetated open channel flow. J. Appl. Fluid Mech. 9 (6), 2865–2875.

Marion, A., Zaramella, M., Bottacin-Busolin, A., 2008. Solute transport in rivers with multiple storage zones: the STIR model. Water Resour. Res. 44, W10406.

Marois, D.E., Mitsch, W.J., Song, K., Miao, S., Zhang, L., Nguyenet, C.T., 2015. Estimating the importance of aquatic primary productivity for phosphorus retention in Florida everglades Mesocosms. Wetlands 35 (2), 357–368.

Mossa, M., 2004. Behavior of non-buoyant jets in a wave environment. J. Hydraul. Eng. 130 (7), 704–717.

Mossa, M., De Serio, F., 2016. Rethinking the process of detrainment: jets in obstructed natural flows. Sci. Rep. 6, 39103.

Mossa, M., Ben Meftah, M., De Serio, F., Nepf, H.M., 2017. How vegetation in flows modifies the turbulent mixing and spreading of jets. Sci. Rep. 7, 6587. http://dx.doi.org/10.1038/s41598-017-05881-1.

Naden, P., Rameshwaran, P., Mountford, O., Robertson, C., 2006. The influence of macrophyte growth, typical of eutrophic conditions, on river flow velocities and turbulence production. Hydrol. Process. 20 (18), 3915–3938.

Nepf, H., Mugnier, C., Zavistoski, R., 1997. The effects of vegetation on longitudinal dispersion. Estuar. Coast. Shelf Sci. 44, 675–684.
Nepf, H., 1999. Drag, turbulence and diffusivity in flow through emergent vegetation. Water Resour. Res. 35 (2), 479–489.
Nepf, H., Ghisalberti, M., White, B., Murphy, E., 2007. Retention time and dispersion associated with submerged aquatic canopies. Water Resour. Res. 43, W04422.
Nepf, H., 2012a. Flow and transport in regions with aquatic vegetation. Annu. Rev. Fluid Mech 44, 123–142.
Nepf, H., 2012b. Hydrodynamics of vegetated channels. J. Hydraul. Res. 50 (3), 262–279.
Nepf, H., Vivoni, E., 2000. Flow structure in depth-limited, vegetated flow. J. Geophys. Res. 105 (C12), 28547–28557.
Nezu, I., Onitsuka, K., 2001. Turbulent structures in partly vegetated open-channel flows with LDA and PIV measurements. J. Hydraul. Res. 39 (6), 629–642.
Okubo, A., 1971. Oceanic diffusion diagrams. Deep Sea Res. 18, 789–802.
Oldham, C.E., Sturman, J.J., 2001. The effect of emergent vegetation on convective flushing in shallow wetlands: scaling and experiments. Limnol. Oceanogr. 46 (6), 1486–1493.
Perucca, E., Camporeale, C., Ridolfi, L., 2009. Estimation of the dispersion coefficient in rivers with riparian vegetation. Adv. Water Resour. 32, 78–87.
Poggi, D., Krug, C., Katul, G.G., 2009. Hydraulic resistance of submerged rigid vegetation derived from first-order closure models. Water Resour. Res. 45, W10442.
Pollen, N., Simon, A., 2005. Estimating the mechanical effects of riparian vegetation on stream bank stability using a fiber bundle model. Water Resour. Res. 41, W07025.
Raupach, M.R., Thom, A.S., 1981. Turbulence in and above plantcanopies. Annu. Rev. Fluid Mech. 13, 97–129.
Raupach, M., Shaw, R., 1982. Averaging procedures for flow within vegetation canopies. Bound. Layer Meteorol. 22, 79–90.
Ricardo, A.M., Di Carlo, S., Franca, M.J., Schleiss, A.J., Sanches, P., Ferreira, R.M.L., 2014. Vortex interaction in patches of randomly placed emergent cylinders. In: Schleiss, A.J., De Cesare, G., Franca, M.J., Pfister, M. (Eds.), River Flow 2014. Lausanne, Switzerland, Taylor & Francis Group, London, pp. 63–69.
Righetti, M., Armanini, A., 2002. Flow resistance in open channel flow with sparsely distributed bushes. J. Hydrol. 269, 55–64.
Righetti, M., 2008. Flow analysis in a channel with flexible vegetation using double-averaging method. Acta Geophys. 56 (3), 801–823.
Rodi W., Turbulence model and their application in hydraulics – a state of the art review, Proceedings of the IAHR Monograph 1984, Balkema, Rotterdam.
Rubol, S., Battiato, I., de Barros, F.P.J., 2016. Vertical dispersion in vegetated shear flows. Water Resource Res. 52, 8066–8080.
Sandercock, P.J., Hooke, J.M., 2011. Vegetation effects on sediment connectivity and processes in an ephemeral channel in SE Spain. J. Arid Environ. 75, 239–254.
Schultz, R.C., Colletti, J.P., Isenhart, T.M., Simpkins, W.W., Mize, C.W., Thompson, M.L., 1995. Design and placement of a multi-species riparian buffer system. Agroforest. Syst 29, 201–226.
Shivpure, V., Bebina Devi, T., Kumar, B., 2016. Turbulent characteristics of densely flexible submerged vegetated channel. J. Hydraul. Eng. 22 (2), 220–226.
Shucksmith, J.D., Boxall, J.B., Guymer, I., 2010. Effects of emergent and submerged natural vegetation on longitudinal mixing in open channel flow. Water Resour. Res. 46, W04504.
Shucksmith, J.D., Boxall, J.B., Guymer, I., 2011. Determining longitudinal dispersion coefficients for submerged vegetated flow. Water Resour. Res. 47, W10516.
Sonnenwald, F.J., Hart, R., West, P., Stovin, V.R., Guymer, I., 2017. Transverse and longitudinal mixing in real emergent vegetation at low velocities. Water Resour. Res. 53, 961–978.
Tanino, Y., Nepf, H., 2008. Lateral dispersion in random cylinder arrays at high Reynods number. J. Fluid Mech. 600, 339–371.
Taylor, GI, 1935. Statistical theory of turbulence. Proc. R. Soc. Lond. Ser. A Math. Phys. Sci. 151 (873), 421–444.
Termini, D., 2013. Effect of vegetation on fluvial erosion processes: experimental analysis in a laboratory flume. Procedia Environ. Sci. 19, 904–911.
Termini, D., 2015. Flexible vegetation behaviour and effects on flow conveyance: experimental observations. Int. J. River Basin Manag. 401–411.
Termini, D., 2016a. Reduction of scouring downstream of a rigid bed by means of a vegetated carpet: experimental investigation in a laboratory flume. Environ. Fluid Mech. 1111–1127.
Termini, D., 2016b. Experimental analysis of the effect of vegetation on flow and bed shear stress distribution in high-curvature bends. Geomorphology.
Termini, D., Sammartano, V., 2012. Morphodynamic processes downstream of man–made structural interventions: experimental investigation of the role of turbulent flow structures in the prediction of scour downstream of a rigid bed. Phys. Chem. Earth 49, 18–31.
Termini, D., 2017. Vegetation effects on cross-sectional flow in a large amplitude meandering bend. J. Hydraul. Res. 55 (3).
Ting, F.C.K., Kirby, J.T., 1994. Observation of undertow and turbulence in a laboratory surf zone. Coast. Eng. 24, 51–80.
Ting, F.C.K., Kirby, J.T., 1995. Dynamics of surf-zone turbulence in a strong plunging breaker. Coast. Eng. 24, 177–204.
Ting, F.C.K., Kirby, J.T., 1996. Dynamics of surf-zone turbulence in a spilling breaker. Coast. Eng. 27, 305–310.
White, B., Nepf, H., 2003. Scalar transport in random cylinder arrays at moderate Reynolds number. J. Fluid Mech. 487, 43–79.
White, B., Nepf, H., 2007a. Shear instability and coherent structures in shallow flow adjacent to a porous layer. J. Fluid Mech. 593, 1–32.
White, B., Nepf, H., 2007b. A vortex-based model of velocity and shear stress in a partially vegetated shallow channel. Water Resour. Res 44 (1), W01412.
Zong, L., Nepf, H., 2012. Vortex development behind a finite porous obstruction in a channel. J. Fluid Mech. 691, 368–391.